ISTITUTO NAZIONALE DI FISICA NUCLEARE

Laboratori Nazionali di Frascati

INFN-23-16-LNF
26 Aprile 2023

Validation procedure of the SM1 Micromegas chambers for the muon spectrometer upgrade of the ATLAS experiment at LHC

Antonelli M.[1], Arcangeletti C.[1], Beretta M.[1], Capitolo E.[1], Cerioni S.[1], Gauzzi P.[2], Lauciani S.[1], Mancini G.[1], Massarotti P.[3], Pileggi G.[1], Paris M.[1], Ponzio B.[1], Putino F.[1], Russo V.[1], Tskhadadze E.[1], Vassilieva T.[1]

[1)] *INFN, Laboratori Nazionali di Frascati, 00044 Frascati, Italy*
[2)] *INFN Sapienza*
[3)] *Università Federico II di Napoli*

Abstract

MicroMegas (MICRO MEsh GAseous Structure) detectors are the new precision tracking detectors installed in the forward muon spectrometer of the ATLAS experiment, composing the New Small Wheel (NSW). The INFN built 32 MicroMegas chambers for the small sector of the NSW (SM1). The validation procedure developed at LNF to ensure the geometry requirements, the gas tightness and guarantee good performance in High Voltage of the SM1 modules is presented in this note.

Published by
Laboratori Nazionali di Frascati

1 Introduction

During the next LHC phases, the luminosity is expected to reach peaks of 5 - 7 times the initial design values and a final integrated luminosity of about 3000 fb^{-1}. The increase of the particle rate is requiring several upgrades of the ATLAS sub-detectors. One the most important upgrade is the replacement of the innermost muon station in the end–caps of the ATLAS experiment (called *Small Wheel*) with the New Small Wheel (NSW)[1], consisting in a completely new detectors technology, the MicroMegas detectors (MM) [2][3], and the small Thin Gas Chamber (sTGC) detectors [4].

MicroMegas chambers is an abbreviation for MICRO MEsh GASeous Structure and it is an innovative design concept for Micro-Pattern Gaseous Detectors first introduced by Charpak and Giomataris during the 1990s [2]. MicroMegas are gas detectors in which a 5 mm gap between two parallel electrodes is filled with a 93 : 7 $Ar : CO_2$ gas mixture and a thin metallic micromesh is placed between the two electrodes, held by pillars with a pitch of few millimetres and a height of about 128 μm (Figure 1). In this way two different region are defined: a *drift region* defined by the drift electrode, where the primary ionisation happens, with a -300 V voltage applied, and the grounded mesh; and an *amplification region* between the mesh and the anode that is done with resistive strips kept at 570 V. In the region the electric field is very high (40 - 50 kV/cm) and the electrons produce avalanches with a gain of the order of 10^4. The thin amplification gap allows a fast ions evacuation (about 100 ns) and allows MM to operate in highly radiated environments. The produced signal is then read by the readout strips capacitively coupled to the resistive ones (pitch of about 400 μm) in order to reduce the performance degradation due to discharges in the detector.

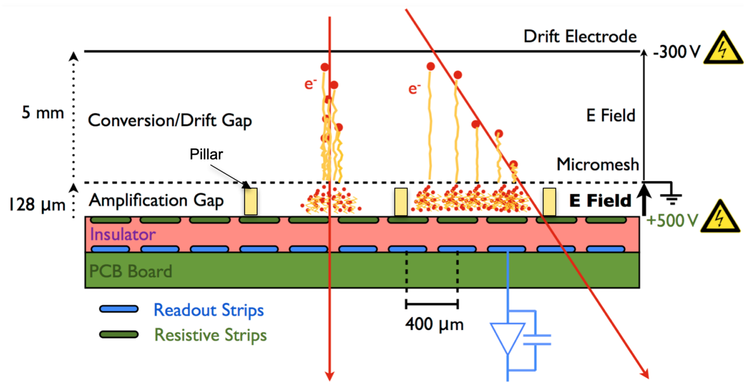

Figure 1: Schematic view of the micromegas detector and the principles of operation.

Figure 2 shows a schematic view of a Micromegas module for the NSW. Each quadruplet is composed of five panels, to have four active gaps. Three out of the five panels (panels 1, 3 and 5 in the figure) are called *Drift panels*, and are made of the drift PCB cathode and meshes. The panels 1 and 5 are the *external* drift panels (or *outer*) while the panel 3 is the *central* one. The cathode layers consist of PCBs with copper layers and they are placed, as for the meshes, on the inner face of the external panels and on both sides of the central. The panels 2 and 4 are called *Readout panels* and the active area is composed by the anode readout PCBs.

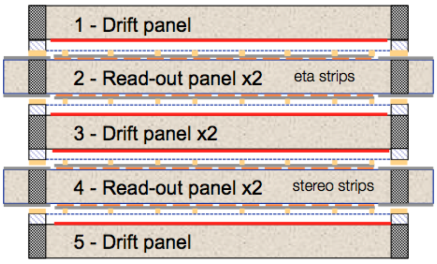

Figure 2: A schematic view of the five panels of a MM quadruplet.

The readout PCB consists of a 500 μm thick FR4 layer on top of which copper strips of 17 μm height are printed via photolitography. The strips are 300 μm wide for all the modules with a pitch of 425 - 450 $\pm$ 20 μm for small and large modules respectively. The shape of the resistive strip foils is almost identical as the readout PCBs. They are composed of a 50 μm thick Kapton® substrate glued on the readout strips, with screen-printed resistive strips, 8-10 μm thick. Figure **??** show the pattern of the resistive strips. It consists of strips congruent to the readout layer, but with an array of bridges connecting each strip alternating with its top or bottom neighbour every 10 mm. This yields a more homogeneous surface resistivity which is less effected by damages than single lines. Finally the strips are interrupted in their centre to divide the surface into two High Voltage sectors, interconnecting all resistive lines. In this way each side of the PCB has a separate high voltage supply line. Consequently, the MM module of type 1 has 10 HV sections in each layer (40 HV sections in total), as schematically shown in Figure 4.

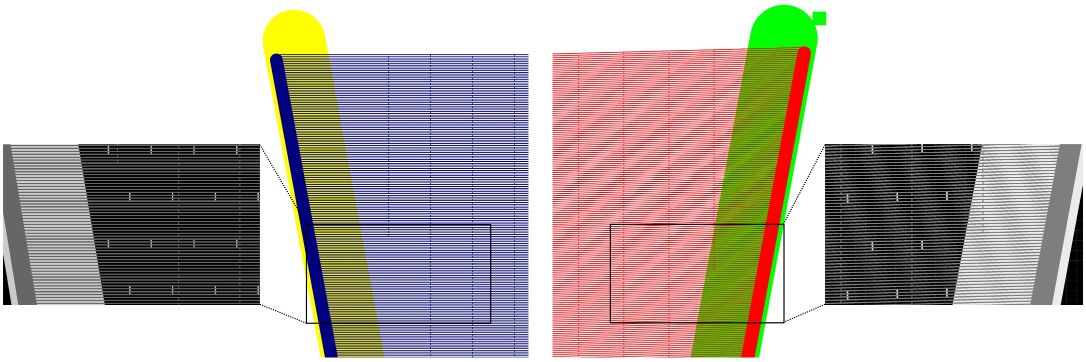

Figure 3: (left) Layout of the PCB resistive strips pattern for an *Eta* (left) and *Stereo* (right) panel close to the panel edge. The insert shows a a more detailed view including the positions and shape of the pillars and the routing of the strips below the coverlay up to the silver line. The resistive connections appear as vertical lines in both figures.

In the quadruplet layout, the strips of the first two layers are parallel to the chamber bases, and almost orthogonal to the bending plane of the tracks in the ATLAS experiment.

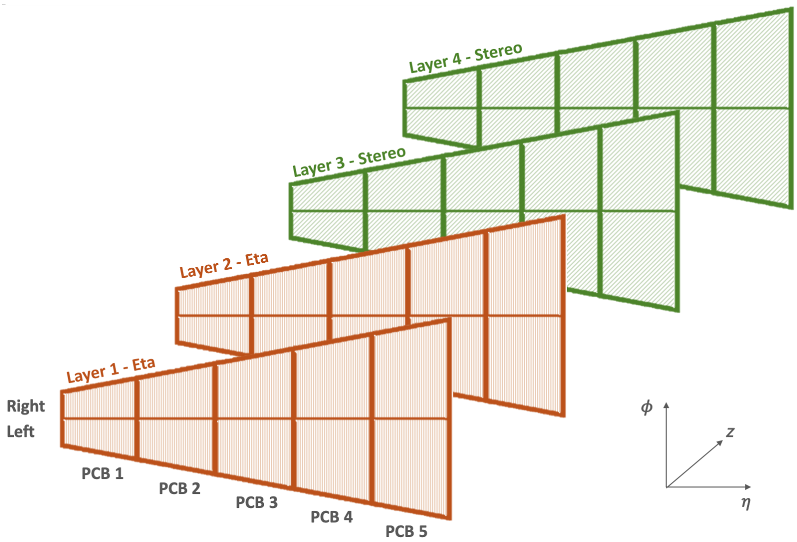

Figure 4: HV schema distribution for SM1 MM module.

The panel that forms these two layers is called *Eta panel*. In the case of the third and fourth layer, formed by the *Stereo panel*, the strips are inclined by $\pm$ 1.5° with respect to the strips of the *Eta panel*. This configuration allows not only a precise determination of the X coordinate, orthogonal to the strips and necessary for the momentum measurement, but also a determination of the second Y coordinate, although with less precision.

Figure 5 shows the layout of one PCB readout board for each type (*Eta* and *Stereo*). Each PCB readout board consists of 512 readout strips, half of them routed to the upper right corner to be readout while the other half, to the bottom left. This scheme balances the load for electronic boards on each side of the detector. The figure shows (highlighted in red circles) also the three coded masks etched on the copper layer along each PCB side. Those masks are know as *Rasnik Mask* [8], or *Rasmask*, and they are used to perform the alignment measurements between the 4 layers, as will be described in Section 2.3.

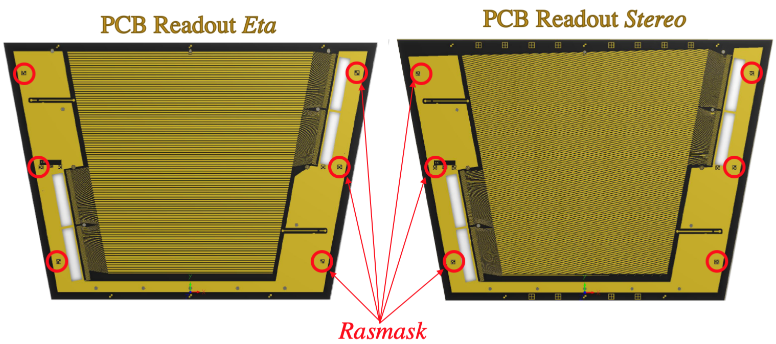

Figure 5: Layout of *Eta* and *Stereo* PCBs. Red circles highlight the three coded masks (*Rasmask*) present on each side of the PCBs.

In this note, an overview of the validation procedure a full SM1 quadruplet developed at LNF is presented.

2 Validation of SM1 Module at LNF

Several quality tests are performed on the Micromegas modules to ensure their performances are in line with the construction requirements.

- *Planarity* of the module, required to be < 100 μm but values up to 200 μm are tolerated, and *thickness* is required to be consistent between the modules.
- *Gas tightness*. It is an important requirement, given that a gas leak in the module can lead to a contamination of the gas mixture with air and water, based on the humidity level. This effect would compromise the performance of the chambers. The ATLAS requirement is that the relative variation of the gas volume inside the chamber in time should be $< 10^{-5}$ Vol/min.
- *Strip alignment* measurement have to be performed to map the mis-alignments or rotations of the readout strips. This is to correct the track reconstruction taking into account of these effects. Mis-alignments < 60 μm are required, and tolerated up to 100 μm.
- *High Voltage stability*. Fundamental test to guarantee the functioning of the chamber at the nominal voltage without discharges. The nominal HV working point is 570 V in Ar:CO_2 93:7 gas mixture and a maximum of 6/40 HV sections not reaching nominal HV are tolerated.

2.1 Planarity and Thickness

This test is performed in the clean room, positioning the quadruplet on the granite table on top of several precise supports (the uniformity of the thickness between the supports has been measured to be within 20 μm), as shown in the scheme of Figure 6a. The support plane represents the reference plane (z=0) for planarity and thickness measurements.

The measurement is made with a Laser Tracker [7]. This tool is based on the laser interferometer to measure relative distances. It works on the principle of light interference in which one beam is used as a reference while the other beam is reflected back from a mirror or retro-reflector at some distance, producing interference. The distance can be calculated from the number of interference fringes, given that the wavelength of the laser is well known.

The laser tracker is first calibrated by taking the supports as the reference plane for the measurement. The module is then positioned on them to start the measurement. Figure 6b shows the laser tracker during the data taking of one module. The laser points to the retro-reflective target, the tool is then moved on the module surface and the height map of more than $\sim$3000 points is built for each side of the module.

A planar fit is performed on the cloud points. Figure 7 shows the measured points and interpolated surface for both side of one module named after the nearest layer of the

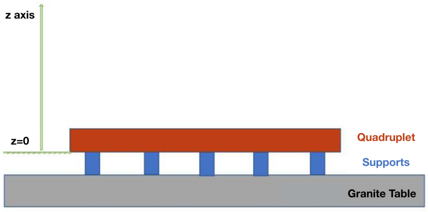

(a) Setup for planarity measurement

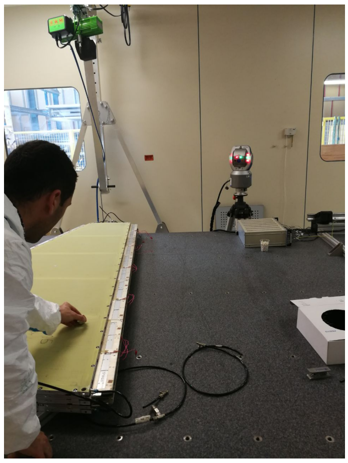

(b) Data acquisition with Laser Tracker

Figure 6: Planarity measurement.

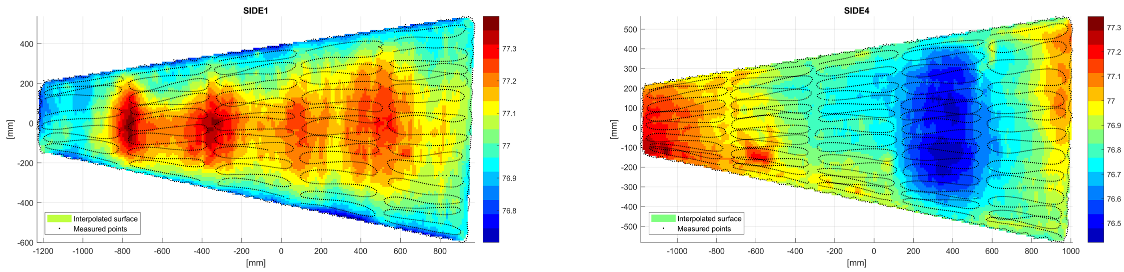

Figure 7: Point clouds obtained with the Laser Tracker and the interpolated surfaces of the two sides of the module for the planarity and thickness measurements.

module. The thickness of the module is then extracted from the mean value of all the measurements and the planarity is taken from the RMS.

A study has been done to estimate the deformation of the modules due to the gas pressure. This test has been performed on one prototype of the final Micromegas SM1 module, called *Doublet* as it was built with just two gas gaps (i.e. with only one readout panel and two external drift panels). Two sets of measurement have been collected, one without overpressure and the other with an overpressure of $\sim$3 mbar.

The results are summarised in Table 1, which show that the difference of the mean thickness $\Delta <$z$>$ of the panel with and without pressure is about 100 μm. The deformation on the external panels is independent on the number of module layers, as it depends only on the overpressure. Therefore the measurement performed on the Doublet can be used as a reference for the Quadruplet. As the SM1 modules have a volume of 40 L and a surface area of 2 m^2, a thickness variation of 100 μm can be translated in a volume variation of 0.2 L. The relative volume variation due to the deformation of the chamber in an overpressure regime is about 0.5 %.

Side 1		Side 2	
Δz (mm)	RMS (mm)	Δz (mm)	RMS (mm)
0.097	0.055	0.107	0.056

Table 1: Results from laser tracker measurements of the Doublet thickness difference with and without pressure.

2.2 Gas Leak Test

The tightness of the module is an important parameter to guarantee the performance of the chamber. This test is performed with the module in horizontal position on the granite table in Clean Room. The gas leak is measured with the *Pressure Drop* technique. The module is over-pressured in a static way (no continuous gas flushing) and then the variation of the pressure in time is measured.

Given the ideal gas law:

$$PV = nRT \ , \tag{1}$$

the gas leak in a given volume V, pressure P and temperature T is due to a variation of the gas mass, related to Δn. The temperature in the clean room roughly constant being controlled within 1 degree and in any case, effects related to temperature variations are taken into account. Then assuming a constant pressure in the chamber during the gas flushing, usually evaluated in terms of L/hour, this mass variation can be expressed as a gas volume variation ΔV.

The ATLAS requirement for the gas leak is expressed in terms of relative variation of the gas volume inside the chamber in time:

$$\frac{\Delta V}{V}\frac{1}{\Delta t} < 10^{-5}\text{min}^{-1} \ . \tag{2}$$

This formula can be translated to relative variation of the pressure inside the chamber with respect to the atmosphere pressure outside the chamber during a pressure drop measurement. In this case, there is no constant gas flushing in the chamber and the pressure variation in the chamber is just due to a possible leak:

$$\frac{\Delta P}{P} = \frac{\Delta V}{V} \qquad \Rightarrow \qquad \text{ATLAS Limit: } \frac{\Delta P}{\Delta t} = 0.64 \text{ mbar} \cdot \text{hour}^{-1} \ , \tag{3}$$

assuming an external pressure P = 1 atm and a constant volume V= 40 L for the SM1 modules. This relation is based on the assumption that the volume of the chamber does not change with the gas flushing. As shown in the previous section, the volume deformation in overpressure condition is about 0.5% of the volume. As such, the effect on the relative variation $\Delta V/V$ is negligible.

The measurement is performed connecting the gas input line of the module to a siringe of 200 mL capacity and the gas output to a sensor to measure the pressure inside the chamber (Figure 8). The value of the initial pressure inside the chamber is taken as reference and then air is injected with the siringe in the chamber until an over-pressure of $\sim$3 mbar is reached. The pressure variation is then monitored together with the temperature.

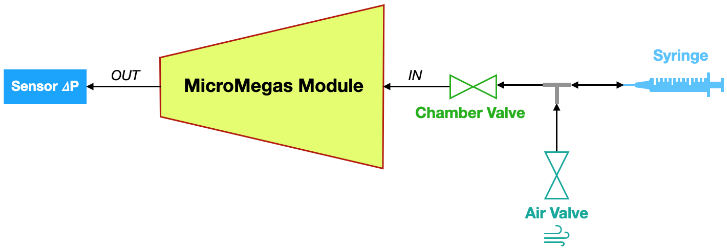

Figure 8: Setup scheme used at LNF to perform the pressure drop measurement.

Figure 9 shows the pressure drop due to the chamber leakage. A linear fit is then performed to extract a measurement of the leakage expressed in terms of mbar/hour. The duration of the measurement is about 15-20 minutes. In this short time range, the temperature variation ΔT is negligible as shown on the bottom panel of the plot in Figure 9, and also its effect on the pressure variation.

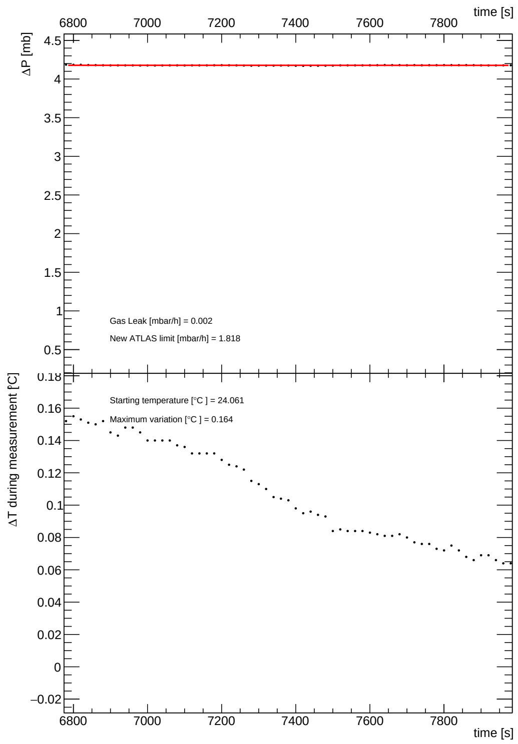

Figure 9: Pressure drop plot to measure the gas tightness of the chamber. The red line represent the linear fit to extrapolate the gas leak measurement. The bottom panel shows the Clean Room temperature variation during the measurement.

2.3 Strip and Panel Alignment

It is very important to measure that displacements and rotations between one PCB and another are below 100 μm to not spoil the detector spatial resolution. In principle every measured offset can be accounted for in the offline track reconstruction, but misalignments can directly affect the trigger performances. For this purpose, many alignment measurements are performed during the construction of MM modules to measure all the possible parameters which can affect the track reconstruction. The as-built parameters to be determined with the alignment measurements are:

- PCB shape parameters: Strip sagitta and elogantions
- PCB alignment in-Layer: PCB translation and rotation and the in-Layer coordinate system
- Layer alignment in-Panel: Layer translation and rotation and the in-Panel coordinate system
- Panel alignment in-Module: Panel translation and rotation and the in-Module coordinate system

From a complete map of any displacements and rotations between the PCB, it is possible to perform a combined fit of all available measurements to reconstruct the full module metrology, which can be used at the muon reconstruction level. These parameters are measured several times with different tools, given that the individual measurement set does not cover the full module metrology.

At LNF, the panel-to-panel alignment is measured after the module assembly. The measurement is performed using a custom-made tool called *4-Rasfork*, based on the *Rasnik* system [8] and developed at Saclay, that is able to measure the relative misalignment of the corresponding PCB on the two panels. The ATLAS requirement on the Panel-to-Panel mis-alignment along the precision coordinate is $\Delta\eta < 100$ μm.

As anticipated in Figure 5, Micromegas PCBs have three coded masks along each PCB side. These masks can be analysed by *Rasnik* system, using a contact CCD (cCCD) coupled with LEDs. This projects the PCBs coded masks onto the cCCD camera. The *Rasnik Mask* (Rasmask) is a chessboard, as shown in Figure 10 with some squares switched from black to white, and other switched from white to black in way to indicate to a camera which part of the mask it is looking at. The images of the masks are analysed by a dedicated LWDAQ software developed by Brandeis University [9]. The software performs the analysis of the rasmask pattern and determines the center of the mask with respect to the cCCD center (image sensor), defining the *rasnik position*. Then the final Rasnik measurement consists of the x and y coordinates of a point in the mask, the magnification of the mask image and the rotation of the mask with respect to the image sensor.

The 4-Rasfork instrument is made of four Rasfork tubes and a circuit of 4 cCCDs with a support block. A Rasfork tube consists of a prism holder, equipped with a prism and a LED circuit, and a tube consisting of 2 half tubes, a lens and a diaphragm at their junction. The light reflected by the rasmasks is guided by the prism, that works in total internal reflection, in the tubes and reaches the cCCD (one for each tube). The measure-

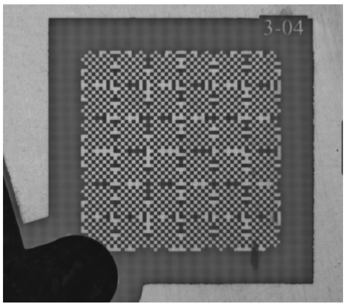

Figure 10: Rasmask installed on the PCBs.

ment setup is shown in Figure 11a. The module is placed on precise shims (the same used for the planarity measurement), so that the Rasfork can be inserted correctly.

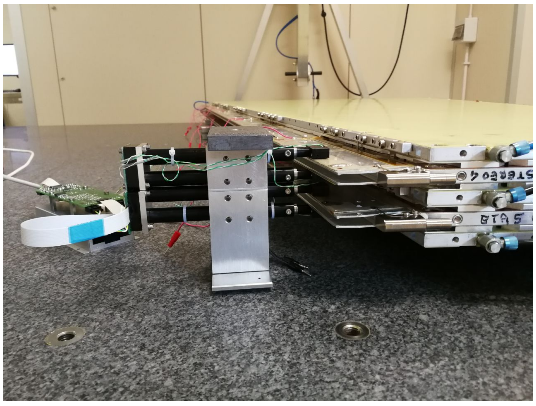

(a) 4-Rasfork setup during a measurement.

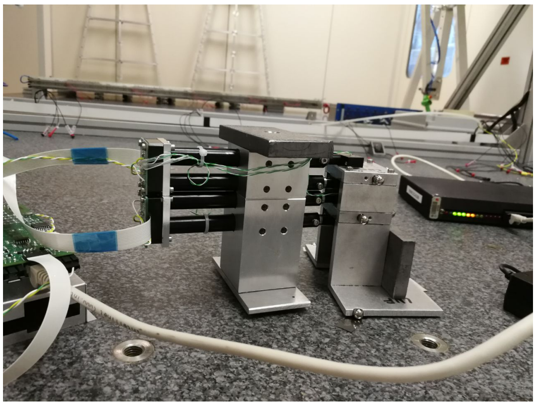

(b) 4-Rasfork during the calibration step at LNF using the Calirasfork.

Figure 11: 4-Rasfork measurement of the panel-to-panel alignment.

4-Rasfork Calibration The Rasfork tool needs to be calibrated, and for this another instrument called *Calirasfork* is used. The Calirasfork is made of a support sitting on 3 balls, holding four glass rasmasks, placed as the masks on the two panel sides. The position and the orientations of the *calimasks* are determined with an accuracy < 3 μm with an optical CMM in Saclay. The calibration procedure is shown in Figure 11b.

4-Rasfork Measurement The Rasfork measurement on the module is performed on all the 30 rasmasks (3 masks each PCB side). The most relevant measurements are the ones performed on the PCB central masks, which is taken as the reference for the relative PCB misalignement, instead the others are sensitive also to possible PCB shape deformations.

An example of map of the mis-alignment $(\Delta x, \Delta y)$ measurements is shown in Figure 12. The y coordinate represents the precision coordinate η in the ATLAS coordinate system.

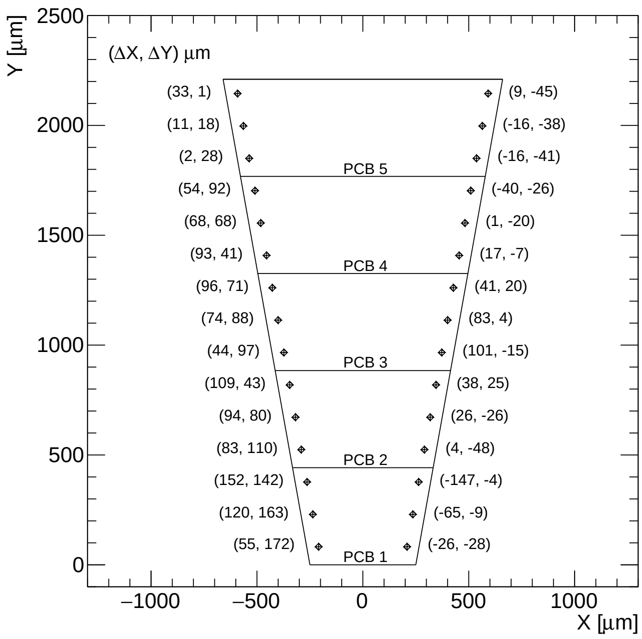

Figure 12: Scheme of the ΔX and ΔY displacement of the readout strips between the Eta and the Stereo readout panel.

2.4 High Voltage Stability Test

The High Voltage stability has been a crucial point of the MM performance during the commissioning phase. Different issues were met during the production of the MM detectors. The solutions for most of them included several additional steps to the MM module construction, as the cleaning procedure and the readout panel passivation.

A further step to improve the HV performance of the chambers is the so-called *conditioning* procedure in High Voltage. This procedure consists in a slow ramp up of the HV voltage applying an initial voltage of 400 V in the amplification region. It is slowly increased until it reaches the nominal working point of 570 V. Once the nominal HV is reached, a long term stability test is performed and the behaviour of the chamber is monitored for several days (also weeks).

HV setup and acquisition The final HV test is performed at Cosmic Ray Stand. All the HV sections are connected to the CAEN Power Supply (PS) SY4527 through the board A7038AP, a Common Floating Return board which allows on-detector grounding, reducing the noise level. In this setup it is possible to power all the 40 Readout HV sections of the module independently, to have a *full-granularity* configuration.

The setting and monitoring of the main HV parameters is performed using the CAEN interface GECO2020. It is the GEneral COntrol Software developed by CAEN for High Voltage boards and systems, which brings the HV control and management via external Host PC using a simple Graphical User Interface (GUI).

The more interesting HV parameters are V_{Mon} (monitored HV) and I_{Mon} (monitored current). These values are constantly recorded by a Data Control System (DCS) developed at LNF. The DCS interfaces with the PS recording data each second using the CAEN HV Wrapper Library functions. Data are transferred to the influx database and Grafana dashboards [1] are used to monitor the trend of the current for each HV section. Figure 13 shows an example of the current monitoring in real-time.

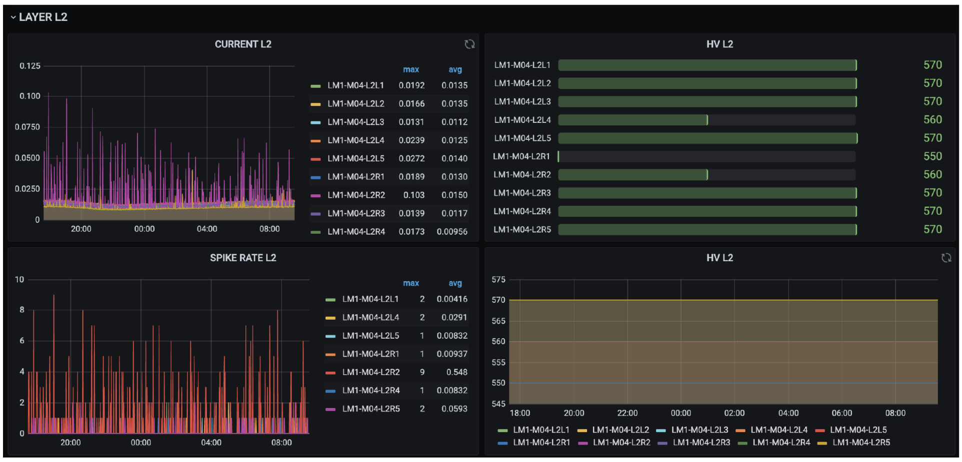

Figure 13: HV monitoring system used at LNF to perform the HV test uses Grafana dashboard to monitor the currents of different HV sections.

Procedure and Criteria The HV test is performed while flushing the chamber with Ar:CO_2 with a gas flux of $\sim$20 L/h. The HV ramp up starts when the gas Relative Humidity (RH) reaches a value $< 10\%$. First, the HV sections are switched on at 100 V to check for major connection problems. Then each section is ramped up at 400 V, and then at steps defined by the following chain:

$$400V \rightarrow 450V \rightarrow 500V \rightarrow 510V \rightarrow 520V \rightarrow 530V \rightarrow 540V \rightarrow 550V \rightarrow 560V \rightarrow 570V \tag{4}$$

The RH is a key parameter in this phase, as high humidity affects strongly the HV behaviour masking eventual underlying issues. The HV test is important also to evaluate which is the maximum HV value that a section can reach, which can be lower than the nominal: 570 V. To identify the maximum HV value for which a section is stable, some acceptance criteria have been defined. These are based on the mean current drawn by the section and on the *spark rate*. The *spark rate* is the frequency in which the current goes above a defined *threshold* (100 nA) in each second. For example, if a section draws a current >100 nA for 6 seconds, it is counted as 6 sparks. The spark rate is defined as the number of sparks per minute.

The HV sections can be flagged as GOOD, CONDITIONING or BAD sections based on the following criteria:

[1] open source analytical and visualisation tool

- **GOOD**: if the section I_{Mon} value is < 10 nA and stable (spark rate ~ 0) the HV value can be ramped up to the next step
- **CONDITIONING**: if the section I_{Mon} value shows *rare instabilities* ($0 <$ spark/min < 6) or few sparks of the order of hundreds nA, the section is left to condition at the corresponding HV value
- **BAD**: if the section I_{Mon} value shows continuous instabilities (spark/min > 6), the HV is lowered until the I_{Mon} value became stable again. The HV could be lowered by 5 V but also by 50 V if needed. The section is left at this HV value for several hours and if it becomes stable, it can be ramped up again following the described procedure.

Figure 14 shows the three different behaviour described above. These criteria are needed also to evaluate if a module has passed the requirements or not.

The ATLAS HV acceptance requirement for a MM module is that the 85% of the sections have to pass the following criteria:

- Nominal HV of 570 V
- Spark Rate < 6/min

If a section fails even one of the requirements, it is not considered as accepted. For the SM1, a module is accepted if at least 34/40 HV sections pass the requirements.

3 Results

In this section, a summary of the QA/QC tests results on SM1 modules performed at LNF is presented. In Figures 15-19, the summary of the QA/QC measurements on the SM1 modules produced are reported.

The planarity measurements results are within the tolerance value of 200 μm for almost all the module. In Figure 15 it is clear that the measurements on the two sides sometimes are quite different. This can be explained by possible defects on the external drift panels, which impact on the measurement on one side, but not on the other. The planarity measurements are indeed sensitive to possible defects on the external drifts and also on the supports used for the measurement.

The gas leak results also show values within tolerances.

The Δy (then $\Delta\eta$ in ATLAS coordinate) alignment results shows a couple of module out of the tolerance. In this case, as explained in Section 2.3, it is possible to fully reconstruct the geometry of the strips using also the other measurements performed on the single panels and PCBs. Then also modules with alignments a bit outside the tolerance can be accepted.

The most important requirement on the HV: at least 85% of the HV sections at 570 V, is respected by all the modules. Nonetheless, Figure 19a shows that Layer 3 and

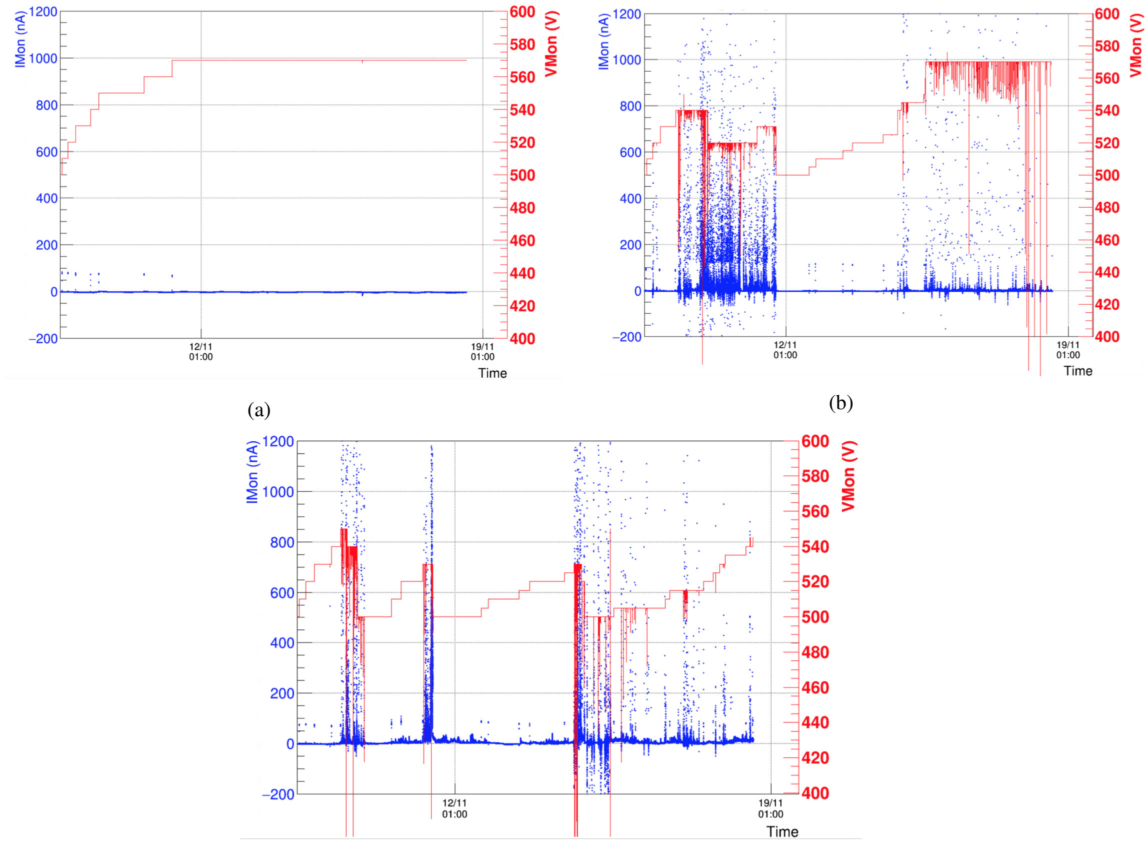

(a)

(b)

(c)

Figure 14: Different HV behaviour. Each plot shows in red the monitored HV (V_{Mon}) and in blue the monitored current (I_{Mon}). An example of a good sector (a), a sector under conditioning (b) and a bad sector (c) are given.

4 (*Stereo* layers) have worst performances with respect to the others (*Eta* layers). The explanation to this behaviour can be found in the layout of the resistive strips, which is different for *Eta* and *Stereo* PCBs.

Looking at the Gerber files of the two type of PCB in Figure 3, it can be seen that the pattern of the interconnection bridges is different between Eta and Stereo. In particular for the Stereo, the first line of interconnections near to the PCB edge ends below the piralux rim, which is 1 cm wide. This means that the shortest strip (above the piralux line) on that PCB is 1 cm long, leading to a lower value of resistance in that area. In such low-resistance regions of the detector, unquenched discharges can easily take place, giving rise to detector instabilities.

A study of the PCB layout and its relation with the resistance has been performed [10] and it shows how the effective resistance seen by any point on the PCB plane depends on the neighbouring resistive strips and on the distance from the closest connection. A simplified model to describe the PCB layout was developed based on the resistive circuit scheme. In Fig. 20 the model has been used to fit the resistance measurements up to the twelfth connection. The measurements and the model clearly show the effect of the connection network, with an overall increase in the resistance moving from the Pyralux rim toward the centre of the RO PCB and drops in correspondence of each interconnection. The fit is able to recover the linear resistivity of the strips, and provides a value of (10.1 $\pm$ 0.7) MΩ/cm, consistent with expectations.

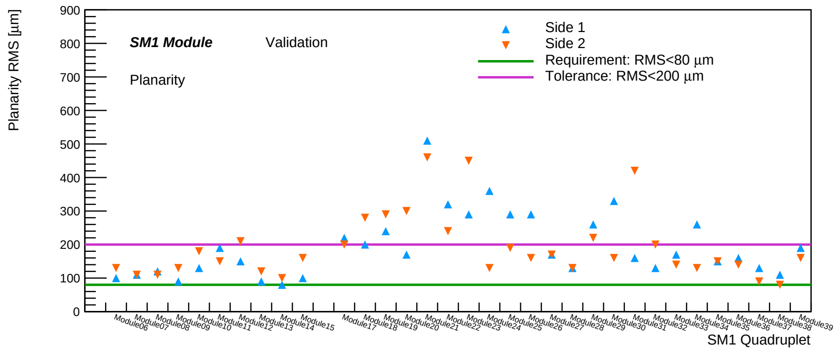

Figure 15: Summary planarity measurements.

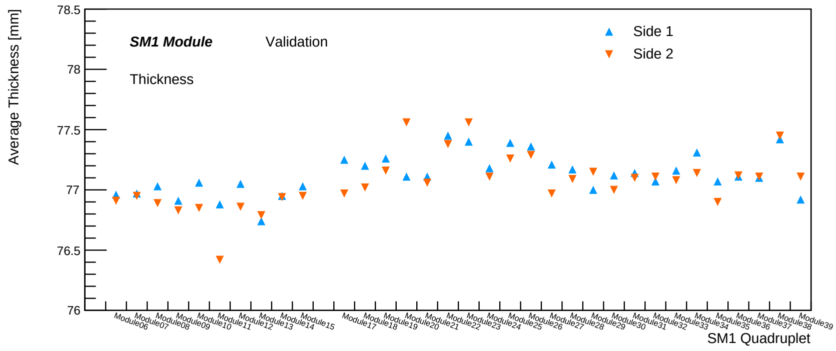

Figure 16: Summary thickness measurements.

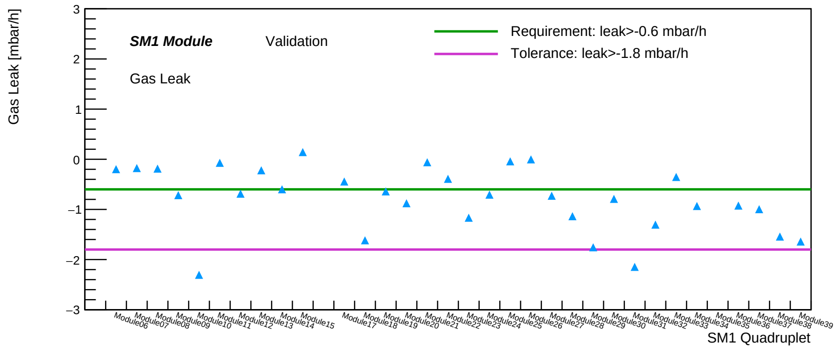

Figure 17: Summary gas leak measurements.

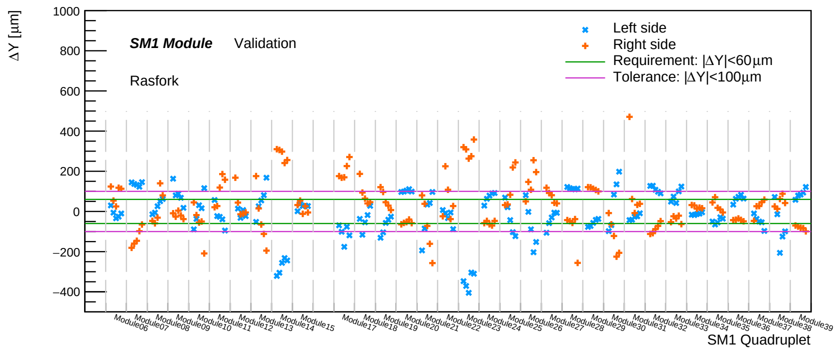

Figure 18: Summary ΔY measurements from rasfork.

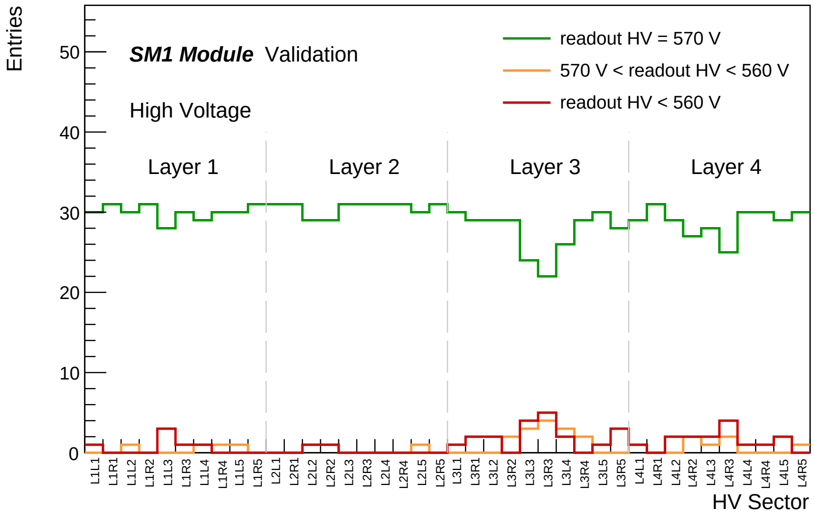

(a)

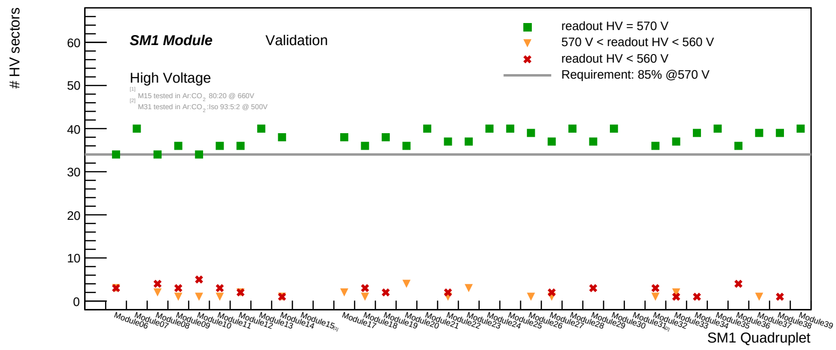

(b)

Figure 19: Summary HV results. Module 15 and Module 31 are not displayed since they were tested in a different gas mixture [10].

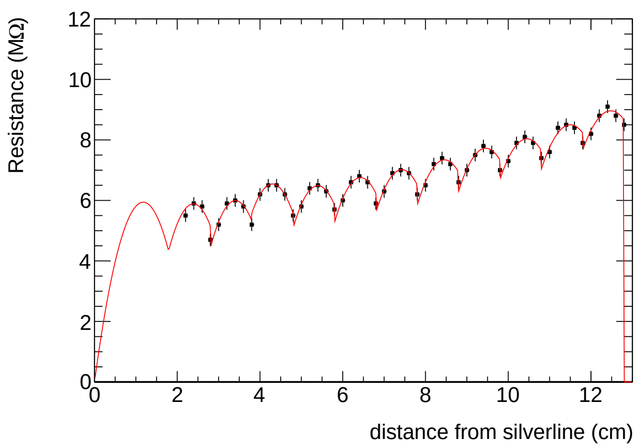

Figure 20: Result of the fit done on the resistance measurements along a resistive strip, as a function of the distance from the silver line up to the twelfth connection, with a simple PCB circuit model.

References

[1] T. Kawamoto *et al.*, New Small Wheel Technical Design Report, CERN-LHCC-2013-006, ATLAS-TDR-020.

[2] Y. Giomataris, P. Rebourgeard, J. P. Robert and G. Charpak, MICROMEGAS: A High granularity position sensitive gaseous detector for high particle flux environments, Nucl. Instrum. Meth. A **376** (1996) 29. doi:10.1016/0168-9002(96)00175-1

[3] M. Iodice [ATLAS Muon Collaboration], Micromegas detectors for the Muon Spectrometer upgrade of the ATLAS experiment, JINST **10** (2015) no.02, C02026. doi:10.1088/1748-0221/10/02/C02026

[4] S. Majewski, G. Charpak, A. Breskin and G. Mikenberg, A Thin Multiwire Chamber Operating In The High Multiplication Mode, Nucl. Instrum. Meth. **217** (1983) 265. doi:10.1016/0167-5087(83)90146-1

[5] T. Alexopoulos, M. Alviggi, M. Antonelli et al., Construction techniques and performances of a full-size prototype Micromegas chamber for the ATLAS muon spectrometer upgrade, Nuclear Inst. and Methods in Physics Research, A (2019), https://doi.org/10.1016/j.nima.2019.04.040

[6] P. Iengo *et al.*, Construction of a large-size four plane micromegas detector, PoS TIPP **2014**, 058 (2014). doi:10.22323/1.213.0058

[7] J. H. Burge, P. Su, C. Zhao, and T. Zobrist, “Use of a commercial laser tracker for optical alignment”, Optical System Alignment and Tolerancing **vol. 6676** (2007), p. 66760E.

[8] M. Beker *et al.*, “The Rasnik 3-point optical alignment system”, JINST **14**, no. 08, P08010 (2019).

[9] Kevan Hashemi, “Rasnik Analysis. Brandeis University”, (2007-2016). url: `http://www.bndhep.net/Devices/RASNIK/Analysis.html`

[10] M. Antonelli *et al.*,“Improvements on the High Voltage stability of the Micromegas chambers for the New Small Wheel upgrade of the ATLAS experiment at LHC”, LNF Note - under publication